Journal of ELECTRONIC MATERIALS, Vol. 42, No. 10, 2013
DOI: 10.1007/s11664-013-2677-x

Simultaneous Formation of Ohmic Contacts on p^+- and n^+-4H-SiC Using a Ti/Ni Bilayer

SUNG-JAE JOO,[1,4] SANGWON BAEK,[2] SANG-CHEOL KIM,[3] and JEONG-SOO LEE[2]

1.—Creative and Fundamental Research Division, Korea Electrotechnology Research Institute, Changwon 642-120, Korea. 2.—Department of Electrical & Electronic Engineering, POSTECH, Pohang 790-784, Korea. 3.—HVDC Research Division, Korea Electrotechnology Research Institute, Changwon 642-120, Korea. 4.—e-mail: sj_joo@keri.re.kr

In this work, Ti/Ni bilayer contacts were fabricated on both p^+- and n^+-4H-SiC formed by ion implantation, and the effects of the Ti interlayer on the contact resistance and interfacial microstructure were studied. Adoption of a thin (10 nm) Ti interlayer resulted in specific contact resistance of 4.8 $\mu\Omega$ cm^2 and 1.3 mΩ cm^2 on n^+- and p^+-4H-SiC, respectively, comparable to the values for contacts using only Ni. Moreover, contacts using Ti/Ni provide a flat and uniform interface between Ni_2Si and SiC, whereas discontinuous, agglomerated Ni_2Si islands are formed without the use of a Ti interlayer. In addition, the Ti interlayer was demonstrated to effectively dissociate the thin oxide film on SiC, which is advantageous for low-resistance, reliable ohmic contact formation. In summary, use of a Ti/Ni bilayer is a promising solution for one-step formation of ohmic contacts on both p^+- and n^+-4H-SiC, being especially suitable for SiC n-channel metal-oxide-semiconductor field-effect transistor (nMOSFET) fabrication.

Key words: 4H-SiC, ohmic, contact, Ti, Ni

INTRODUCTION

Ohmic contacts with low resistance are essential for optimal performance of power semiconductor devices, and the contact formation process should be simple and inexpensive for practical use. In this regard, Ni is the most preferred metal for ohmic contacts on n-type SiC[1–3] due to its low contact resistance as well as the simplicity of the contact formation process. However, Ni is not generally favored for p-type ohmic contacts because it has a work function of 5.15 eV, whereas a metal with a work function higher than 6 eV is required on p-type 4H-SiC to obtain ohmic contacts with Schottky barrier height lower than 1 eV.[3] Instead, Al-based alloy systems, such as Al-Ti,[4–9] Ni-Al,[10,11] and Ni-Ti-Al,[10] are widely studied, and Al is regarded as an essential element to obtain low-resistance p-type ohmic contacts. However, in these cases, p- and n-type ohmic contacts are optimized separately by using different metals and processes, which is complex and costly. Moreover, junction spiking was reported in study of Al/Ti contacts on SiC,[4,9] making practical use of Al-based alloy very difficult in terms of contact reliability. Therefore, Al-based alloy contacts are not yet a mature process and should be optimized for drastic improvement of the contact morphology.

Replacing Al in p-type contacts and utilizing the same metal, e.g., Ni, for both types of contacts would enable a very simple fabrication process, but at the cost of an increase in the resistance of the p-type contact. However, in some cases [for example, 4H-SiC n-channel metal-oxide-semiconductor field-effect transistors (nMOSFETs)] this tradeoff may be acceptable, as long as the high resistance of the p-type ohmic contact is not critical for device operation; in fact, there have been reports on 4H-SiC nMOSFET fabrication[2] and process development[12] using a Ni-only contact scheme.

Although the conventional Ni contact has many great advantages, it also has drawbacks, such as the

(Received March 4, 2013; accepted July 3, 2013; published online July 30, 2013)

formation of rough interfaces with voids,[3,13] that raise concerns about the stability and reliability of the contacts under harsh environments.[3,14] Therefore, it is highly desirable to address the structural shortcomings of Ni contacts using a simple method while preserving their superior electrical properties. To address the structural shortcomings of Ni contacts, we investigated the use of Ti/Ni (where "/" denotes the deposition sequence) contacts to simultaneously form *p*- and *n*-type ohmic contacts on highly doped 4H-SiC substrates.

Ti was chosen for this study because it is one of the most frequently used metals for silicide contacts on SiC[3] as well as for conventional Si devices;[15] i.e., Ti is proven to form reliable low-resistance ohmic contacts. Also, Ti exhibits good adhesion to both Si and SiC, and the formation of a smooth interface was previously reported.[4,16] Therefore, Ti is expected to be used with Ni for realization of reliable ohmic contacts on SiC.

Ti-Ni alloy contacts have been previously studied, with good ohmic properties reported for such contacts on *n*-type 4H-SiC,[16] *p*-type 4H-SiC,[17,18] and *n*-type 6H-SiC.[19] However, to the best knowledge of the authors, there has been no report on simultaneous formation of *p*- and *n*-type ohmic contacts on highly implanted 4H-SiC using the Ti/Ni bilayer system. In this study, we fabricated Ti/Ni ohmic contacts on p^+- and n^+-implanted 4H-SiC, and the specific contact resistances (SCRs) were compared with those of Ni contacts. Also, these samples were analyzed using field-emission transmission electron microscopy (FETEM) and x-ray diffraction (XRD) to elucidate the structural differences between the Ni and Ti/Ni contacts.

EXPERIMENTAL PROCEDURES

Commercial highly doped 4H-SiC substrates (4° off-cut from the [0001] direction, Si-face, resistivity: ~0.02 Ω cm) with lightly doped *n*-type epitaxial layers (thickness: ~12 μm, N_d: ~5.0×10^{15} cm^{-3}) were used in our experiments after dicing to size of 10 mm × 10 mm. The linear transfer length method (LTLM) was used in this study, and Fig. 1a shows a schematic top-view diagram of the LTLM pattern. The spacing between adjacent rectangular contacts (*s* in Fig. 1a) was varied from 5 μm to 25 μm.

The first step of sample preparation involved growth of a thin (10 nm) oxide by thermal oxidation at 1150°C after RCA cleaning,[20] which consists of treatment in 1:1:5 solution of $NH_4OH + H_2O_2 + H_2O$ at 80°C (SC1 clean), short immersion in 1:50 solution of $HF + H_2O$, and final cleaning in 1:1:6 solution of $HCl + H_2O_2 + H_2O$ at 80°C (SC2 clean). Subsequently, a series of implantation steps at substrate temperature of 500°C were implemented to form highly doped regions on the surface. For *p*-type ohmic contact samples, rectangular regions were first patterned by lift-off of the Ti (10 nm)/Au (1 μm) evaporated bilayer, followed by high-dose Al-ion implantation with multiple energies (total dose: ~3.6×10^{15} cm^{-2}, implantation energy: 20 keV to 220 keV) to create p^+-doped regions ($N_{A,max}$: ~1.0×10^{20} cm^{-3}, junction depth x_{jp}: ~600 nm). Next, the periphery of the p^+ regions was etched for electrical isolation of the contact to trench depth (d_t) of approximately 1.2 μm using an Oxford Plasmalab System 100 reactive-ion etching (RIE) instrument utilizing CF_4 and O_2 gases to etch SiC and a patterned Ni film as a hard mask to define the region of etching. For the *n*-type ohmic contact samples, the entire area of the *n*-epilayer was first converted to *p*-type by multiple-energy blanket Al implantation to depth of approximately 1 μm, followed by formation of highly doped n^+ regions by multiple-energy N implantation (total dose: ~1.7×10^{15} cm^{-2}, implantation energy: 20 keV to 80 keV, $N_{D,max}$: ~1.0×10^{20} cm^{-3}, junction depth x_{jn}: ~230 nm). As with the *p*-type samples, a Ti (10 nm)/Au (1 μm) lift-off process was also used to form the n^+ implantation mask, and trenches with depth d_t of approximately 1.2 μm were formed around the n^+-implanted regions for electrical isolation. Subsequently, the implanted samples were spin-coated with photoresist (AZ5214E) after oxide wet etching, then annealed at 1700°C for 60 min in Ar ambient to activate the dopants and repair lattice damage. During this high-temperature annealing, which is a frequently used method for SiC device processing,[21] the photoresist became thermally converted into a carbon capping layer that prevents Si sublimation from the SiC surface.

After activation annealing, the carbon capping layer was removed by sacrificial dry oxidation and an oxide strip in diluted HF, followed by cleaning of the samples using SC1 and SC2 methods. Next, a thermal oxide layer was grown again at 1150°C to produce approximately 50-nm-thick SiO_2 on the SiC surface. The LTLM contact openings were defined by photolithography, followed by RIE using CF_4 and O_2 gases, as described above. The etching conditions for the formation of the contact openings were primarily adjusted so that the thermal oxide (50 nm) on SiC was completely etched away, but in some cases the etching was deliberately designed to leave a thin (approximately 10 nm) oxide layer to block the reaction between the contact metals and the SiC during the rapid thermal annealing (RTA) process. As is well known, Ti can reduce SiO_2 at elevated temperatures,[22] so it is anticipated that the Ti/Ni system can still form stable ohmic contacts even when incomplete contact etching leaves a thin remnant oxide layer on the SiC surface. Immediately after the contact regions were exposed by RIE, the samples were loaded into an e-beam evaporation chamber (base pressure ~5×10^{-7} Torr) with the photoresist pattern intact, and thin Ti (10 nm) and Ni (20 nm) films were sequentially deposited without intentional heating of the samples. After evaporation, the Ti/Ni bilayer was patterned by a lift-off process in acetone. For comparison, reference samples using only Ni

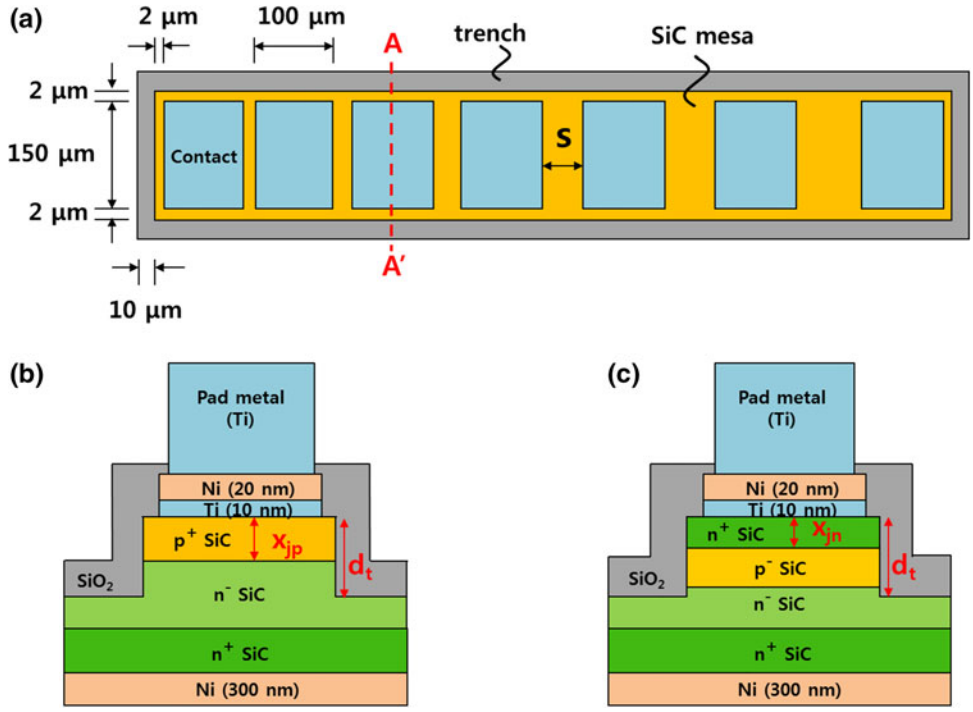

Fig. 1. (a) Schematic top-view diagram of the LTLM pattern, and cross-sectional diagrams along A–A′ of the (b) Ti/Ni p^+ and (c) Ti/Ni n^+ contacts (not to scale).

(20 nm) were also prepared. Thick (300 nm) Ni films were sputtered on the backside of the samples for backside body contact, then the reaction between the metal and SiC was induced by RTA in N_2 atmosphere at either 950°C or 1000°C, the duration of which was varied from 60 s to 120 s. As the last step, 700 nm of Ti was evaporated and patterned on the front side to form the LTLM contact pads. Figure 1b and c show the final structures of the p^+ and n^+ contacts using the Ti/Ni bilayer, respectively.

Current–voltage (I–V) characterization of the LTLM samples was performed using a HP 4156 system. The SCR was extracted by following the LTLM procedure,[3] and over 10 data points were collected for each process condition to obtain statistically meaningful values. XRD data were collected using a PANalytical X'Pert Pro MPD model (Cu K_α radiation, $\lambda = 0.15418$ nm), equipped with incident optics comprising a 0.04-radian Soller slit, a 0.02-mm Ni filter, and a fixed-divergence slit (1/4° divergence), and receiving optics comprising a fixed-divergence antiscatter slit (1/4° divergence), a 0.02-mm Ni filter, a 0.04-radian Soller slit, and a 256-channel solid-state detector. The XRD data were obtained at 40 kV, 30 mA using a θ–2θ scan (typical step size: 0.005°, scan range: 20° to 100°, scan speed: 0.01°/s) as well as low-angle incidence diffraction (incidence angle $\Omega = 5°$). A JEOL JEM-2100F FETEM, with a 200 kV acceleration voltage and a ZrO/W(110) Schottky emitter, was utilized to obtain detailed information about the microstructure and chemical composition at the interfaces by high-angle annular dark-field (HAADF) imaging, energy-dispersive spectroscopy (EDS), and electron energy-loss spectroscopy (EELS).

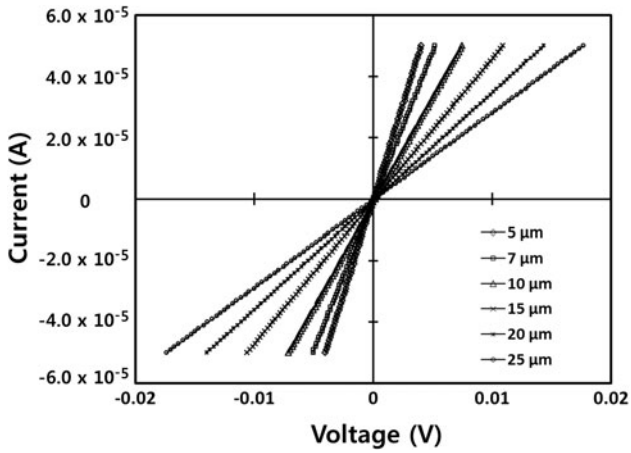

Fig. 2. Current–voltage (I–V) characteristics of ohmic contacts using Ni (RTA: 950°C, 120 s) versus the spacing between the LTLM contacts.

RESULTS AND DISCUSSION

Electrical Measurements

Figure 2 shows the I–V data of the Ni contact on the implanted n-type 4H-SiC, which was annealed at 950°C for 120 s, with varying contact spacing. The data points for each of the contact spacings are perfectly fitted with a straight line, which confirms

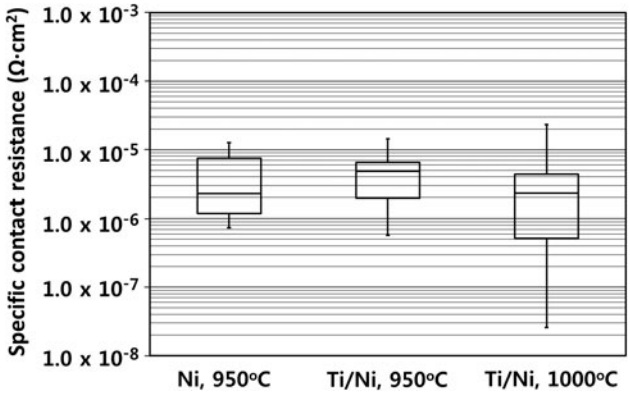

Fig. 3. Box plots of the SCR of n^+ ohmic contacts using Ni or Ti/Ni.

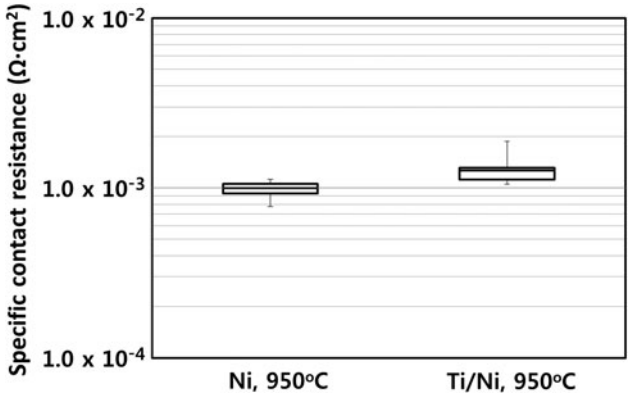

Fig. 4. Box plots of the SCR of p^+ ohmic contacts using Ni or Ti/Ni annealed at 950°C.

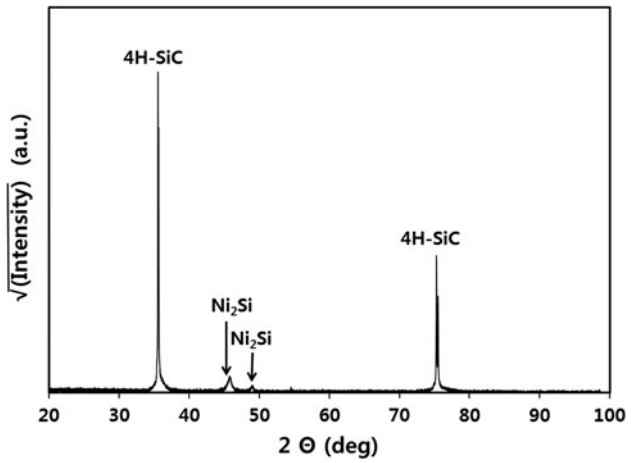

Fig. 5. XRD pattern of Ni on SiC annealed at 950°C.

that ohmic contacts were formed by using RTA at 950°C, and the median of the SCR is approximately 2.3 $\mu\Omega$ cm^2, as shown in the box plot of Fig. 3. In the case of Ti/Ni contacts, a median of approximately 4.8 $\mu\Omega$ cm^2 was obtained at the same RTA temperature (950°C) with shortened RTA time of 60 s, which is approximately twice as high as that of a Ni contact, but the quartile deviation of the data was reduced. The SCR of the Ti/Ni contact is lowered to 2.3 $\mu\Omega$ cm^2 (median) by raising the RTA temperature to 1000°C, but this is accompanied by undesirable widening of the spread in the data. In our study, Ti/Ni contacts did not exhibit lower resistances than the Ni contacts, which can be explained by the fact that Ni itself is already an excellent material for the formation of low-resistance n^+ ohmic contacts on SiC,[1,3] thus leaving little room for dramatic improvements of the electrical properties. Nevertheless, good SCR values of 2.3 $\mu\Omega$ cm^2 to 4.8 $\mu\Omega$ cm^2 were obtained by using Ti/Ni contacts for RTA temperatures in the range of 950°C to 1000°C, so we focused on the original objective of developing a new method to improve the interface morphology while minimizing the increase of the SCR value.

For fixed RTA temperature of 950°C, the Ni and Ti/Ni p-type ohmic contacts exhibited comparable SCR values of approximately 1.0 mΩ cm^2, as shown in Fig. 4. The SCRs of the Ni and the Ti/Ni contacts were 1.0 mΩ cm^2 and 1.3 mΩ cm^2, respectively, demonstrating that Ni contacts exhibited lower SCR values on p^+-implanted SiC as well. The high SCR values of the p^+ ohmic contacts were expected due to the formation of a high Schottky barrier and the low ionization rate of p-type dopants at room temperature when forming metal contacts on p-type SiC.[3] As a viable solution to this fundamental problem, the Al/Ti contact has been widely studied for the formation of SiC p^+ contacts, with favorable SCR values in the range of 10^{-4} Ω cm^2 to 10^{-6} Ω cm^2 reported.[3–7,9] In this approach, Al is indispensable to obtain low SCR, and the effect of the Al content in the Al-Ti alloy on the SCR and the interface morphology has been thoroughly studied.[5,6,9] However, adoption of Al is not compatible with the Ni-based n^+ ohmic contact process, and p^+- and n^+-contacts should be fabricated separately using different metals. Moreover, pitting on the SiC surface has been observed after chemical etching of the Al/Ti layer,[4,9] which can degrade the contact reliability. Similar to Ni contacts, the uneven interface morphology remains the major challenge for practical application of Al-based p^+ contacts. Considering the absence of Al in the contacts studied here, the SCR values of the Ti/Ni p^+ contacts shown in Fig. 4 are acceptable, especially for a common contact on the n^+ source and the p-well regions of SiC nMOSFETs.[2] The major advantage of the Ti/Ni system is undoubtedly the simplicity of the contact formation process. Therefore, we believe that Ti/Ni p-type ohmic contacts have their own merits and applications.

Microstructural Analysis

Figure 5 shows the XRD θ–2θ scan of the Ni blanket thin (20 nm) film on SiC annealed at 950°C

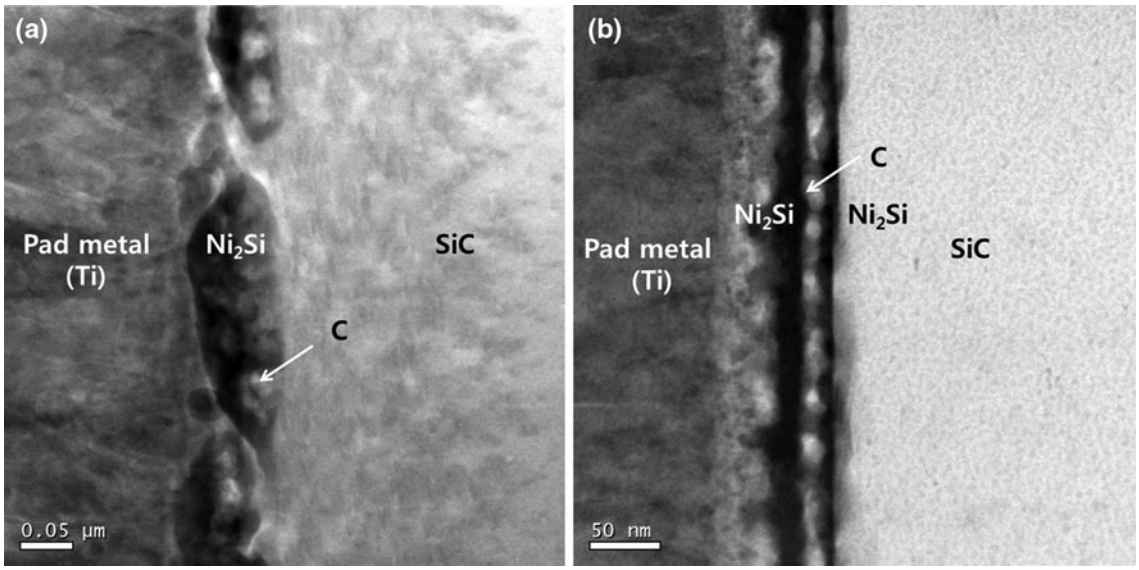

Fig. 6. Bright-field TEM cross-sectional images of contacts using (a) Ni and (b) Ti/Ni.

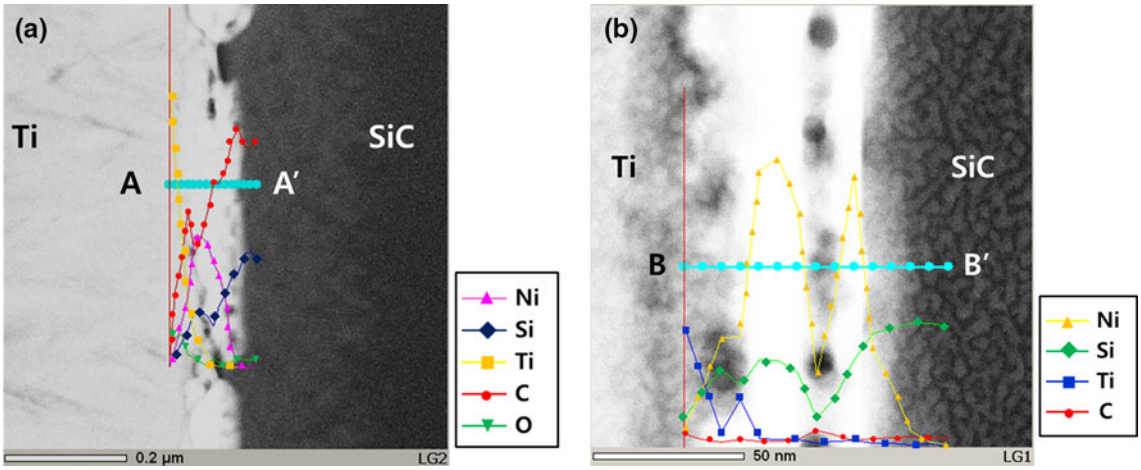

Fig. 7. Cross-sectional TEM HAADF images and distribution of elements obtained by EDS of the contacts using (a) Ni and (b) Ti/Ni.

for 120 s. The peaks from the Ni_2Si phase are clearly identified, and no other phases are discernible. The XRD data from the Ti/Ni samples were almost the same as those in Fig. 5, and it was difficult to distinguish between the Ni and Ti/Ni samples by XRD analysis alone. Considering the weak signal from the thin reacted layer, glancing-angle XRD (incidence angle $\Omega = 5°$) was also implemented, but similar results were obtained and no further information was available from the XRD data. Therefore, TEM analysis was used to obtain detailed information about the microstructure of the contact interfaces.

Figure 6 shows cross-sectional bright-field (BF) TEM images of the (a) Ni contact and (b) Ti/Ni contact. These images clearly demonstrate that the Ti/Ni contact exhibits a smooth and flat interface with the SiC, whereas the Ni contact shows a rough and uneven interface due to Ni agglomeration during the RTA process. The stoichiometry of the nickel silicide phase indicated in Fig. 6 was determined from the XRD pattern in Fig. 5, which shows characteristic peaks of Ni_2Si.[10,19,23,24] Figure 7 displays the HAADF images of the Ni and Ti/Ni contacts shown in Fig. 6 with the distribution of elements (Ni, Si, Ti, and C) superposed on them, which were obtained by EDS in TEM along the straight lines A–A′ and B–B′, respectively. Figure 7b clearly demonstrates that Ni diffused through the Ti layer and reacted with SiC to produce a Ni_2Si interfacial layer. Also, a carbon-rich zone is embedded in the middle of the Ni_2Si layer as a consequence of carbon precipitation, and Ti is located away from the SiC. The reversal of the layer sequence in the annealed SiC/Ti/Ni system has also been reported previously,[16,24] being explained by the significantly

higher reactivity and mobility of Ni than any of the other elements in the diffusion-controlled reaction zone with SiC.[24–26]

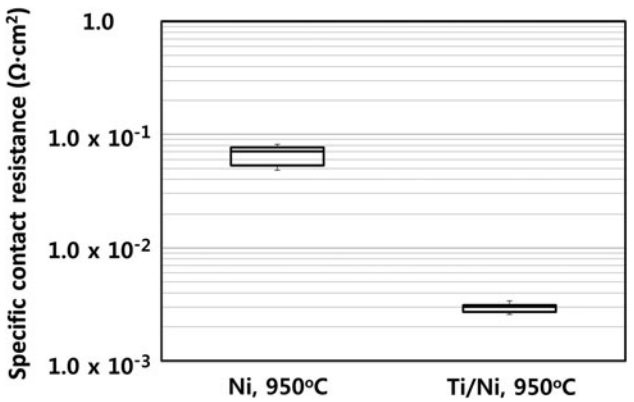

Fig. 8. Box plots of the SCR of p^+ ohmic contacts using Ni or Ti/Ni (annealed at 950°C) when a thin SiO_2 layer (~10 nm) is present in the contact windows due to incomplete dry etching.

Comparing the cross-sectional images, it is notable that the Ni contacts exhibit lower resistances despite the poor interface morphology. Also note that, in Fig. 7, the carbon distribution is different for the different types of contact: for the Ni contact, the carbon concentration is a maximum at the Ni_2Si–SiC interface and decreases monotonically towards the outside, whereas for the Ti/Ni contact, the carbon atoms are predominantly located in the middle of the Ni_2Si as precipitates, and a concentration gradient is not clearly observed. The underlying mechanism of the low SCR in the Ni ohmic contacts is still under debate, and the role of carbon is also inconclusive.[1,3,27] However, referring to a recent study on the formation of a Ti/Al contact on *p*-type 4H-SiC,[28] the key point of ohmic contact formation is an epitaxial, coherent, and atomically ordered interface, and an atomic layer of carbon captured at the interface is predicted to decrease the contact resistance by lowering the Schottky barrier height and enhancing quantum electron transport.

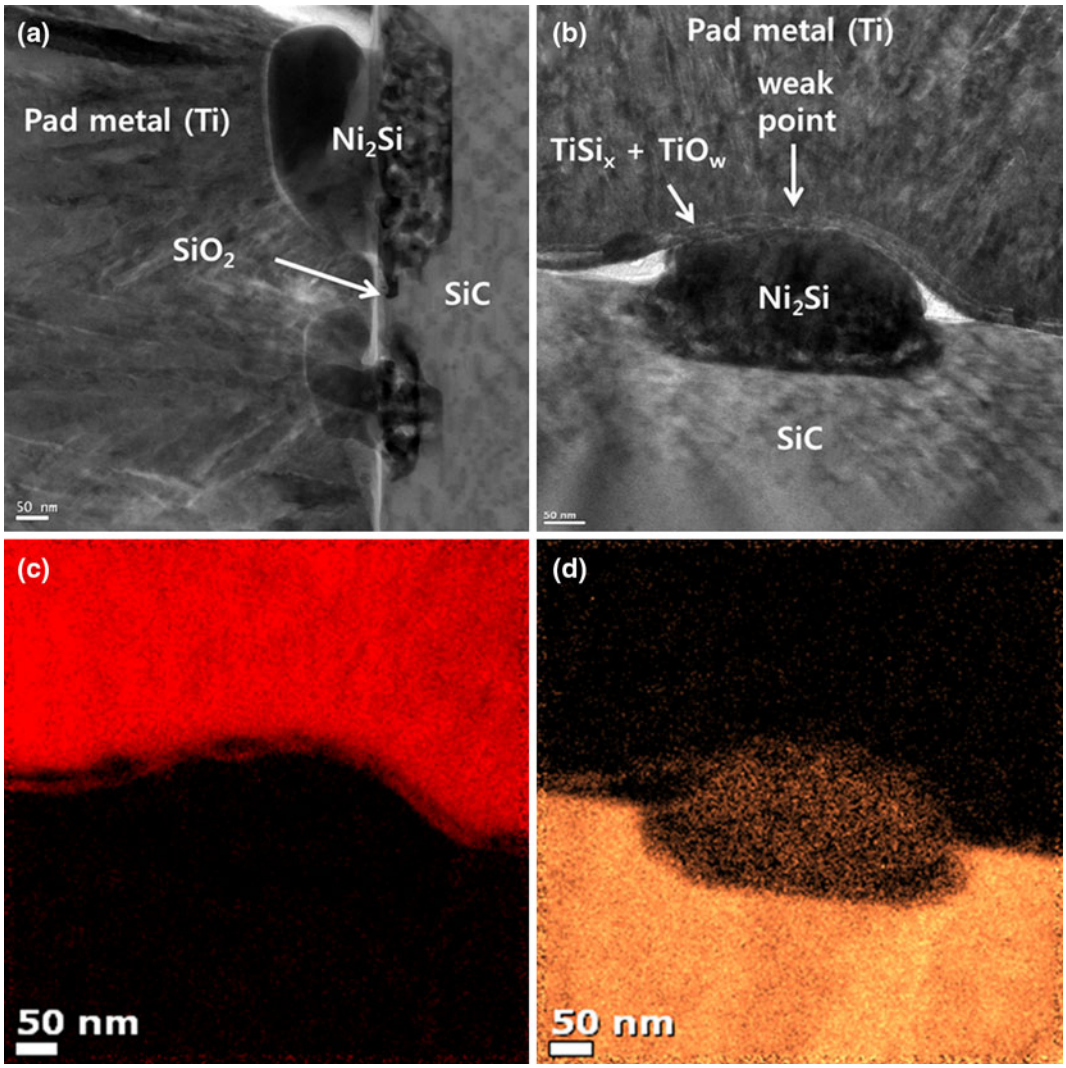

Fig. 9. Bright-field TEM cross-sectional images of contacts (annealed at 950°C) using (a) Ni and (b) Ti/Ni when a thin oxide (~10 nm) remained in the contact windows due to incomplete dry etching. EELS element maps for (c) Ti and (d) Si in this Ti/Ni contact.

We hypothesize that the difference in contact resistance between the Ni and Ti/Ni contacts in this study may be closely related to the different behaviors of carbon, but in-depth research is required to draw a definite conclusion.

The TEM images shown in Figs. 6 and 7 suggest that the thin Ti layer prevented Ni agglomeration, thus making diffusion of Ni through the Ti interlayer proceed uniformly. A similar observation, reported in the field of metal–ceramic composites, indicates that Ti promotes wetting as well as interfacial reaction of Ni on SiC, which results in rugged metal coating on SiC ceramics.[29] This lack of agglomeration clearly demonstrates the advantages of using a thin Ti interlayer for Ni-based ohmic contacts on SiC.

Furthermore, adoption of the Ti interlayer provides an additional benefit of eliminating thin residual SiO_2 in the contact windows. Figure 8 displays the SCRs of the *p*-type ohmic contacts after the RTA process when a thin SiO_2 layer (~10 nm) exists on the SiC surface before metal deposition, as described earlier. When Ni is used, the SCR is approximately 70 mΩ cm^2, which is 70 times higher than the normal value shown in Fig. 4. However, the Ti/Ni contact exhibits a much lower SCR of approximately 3.0 mΩ cm^2, and the SCR increased only 2.3 times due to the presence of the remnant SiO_2.

This relatively modest increase in the SCR is explained by the different microstructures of the interfaces, as shown in Fig. 9. The cross-section of the Ni contact (Fig. 9a) is characterized by irregular arrays of Ni_2Si islands, and remaining area is still covered by the thin oxide film, which cannot contribute to electrical conduction. The TEM image in Fig. 9a suggests that reactive Ni has penetrated through the thin oxide at weak spots, such as pinholes or defective sites, and has reacted with SiC to produce Ni_2Si islands. However, in the presence of the Ti interlayer, Ti and SiO_2 reacted to produce $TiSi_x$ and oxygen-containing Ti (solid solution), TiO_w,[22] as shown in Fig. 9b. Consequently, intimate contact of $TiSi_x$ with SiC is achieved over the entire area, as confirmed by the EELS mapping of Ti and Si shown in Fig. 9c, d. Also, we observed formation of Ni_2Si islands beneath the $TiSi_x/TiO_w$ layer in Fig. 9b, which was formed by penetration of agglomerated Ni through the weak points of the $TiSi_x/TiO_w$ layer. This result suggests that the Ti interlayer may lose its permeability and wettability to Ni as it reacts with SiO_2, which leads to Ni agglomeration and local formation of Ni_2Si islands, instead of uniform Ni diffusion through Ti.

CONCLUSIONS

Use of Ti/Ni bilayer contacts for simultaneous formation of ohmic contacts on p^+- and n^+-implanted 4H-SiC was investigated, and the SCR and microstructure of such bilayer contacts were compared with those of Ni-only contacts. Although the Ti/Ni contacts exhibit slightly higher SCRs than the Ni contacts, the interface morphology is very flat and uniform, whereas the Ni contacts exhibit a rough interface due to agglomeration. The remarkable improvement of the interface morphology is ascribed to the role of the Ti interlayer in promoting Ni wetting on Ti, thus enabling the Ni diffusion and Ni–SiC reaction to proceed uniformly. In addition, the Ti interlayer was demonstrated to dissociate thin interfacial SiO_2 during the RTA process, and the Ti/Ni bilayer enables low-resistance ohmic contacts even when the SiC surface is covered by a thin SiO_2 film, which is quite advantageous for enhancing the reliability of the ohmic contact formation process. In conclusion, the Ti/Ni contact scheme is a viable technique to replace the conventional Ni contact, because the structural weaknesses of the Ni contact are eliminated with a minimum trade-off in the electrical properties.

ACKNOWLEDGEMENTS

This work was funded by the Ministry of Knowledge Economy of Korea (Project Code Number: 12-02-N0401-06).

REFERENCES

1. S. Tanimoto, M. Miyabe, T. Shiiyama, T. Suzuki, H. Yamaguchi, S. Nakashima, and H. Okumura, *Mater. Sci. Forum* 679–680, 465 (2011).
2. S.-H. Ryu, S. Krishnaswami, M. O'Loughlin, J. Richmond, A. Agarwal, J. Palmour, and A.R. Hefner, *IEEE Electron. Dev. Lett.* 25, 556 (2004).
3. F. Roccaforte, F. La Via, and V. Raineri, *Int. J. High Speed Electron. Syst.* 15, 781 (2005).
4. J. Crofton, L. Beyer, J.R. Williams, E.D. Luckowski, S.E. Mohney, and J.M. Delucca, *Solid-State Electron.* 41, 1725 (1997).
5. J. Crofton, S.E. Mohney, J.R. Williams, and T. Isaacs-Smith, *Solid-State Electron.* 46, 109 (2002).
6. O. Nakatsuka, T. Takei, Y. Koide, and M. Murakami, *Mater. Trans.* 43, 1684 (2002).
7. F. Moscatelli, A. Scorzoni, A. Poggi, G.C. Cardinali, and R. Nipoti, *Semicond. Sci. Technol.* 18, 554 (2003).
8. B. Pécz, L. Tóth, M.A. di Forte-Poisson, and J. Vacas, *Appl. Surf. Sci.* 206, 8 (2003).
9. B.J. Johnson and M.A. Capano, *Solid State Electron.* 47, 1437 (2003).
10. R. Konishi, R. Yasukochi, O. Nakatsuka, Y. Koide, M. Moriyama, and M. Murakami, *Mater. Sci. Eng.* B98, 286 (2003).
11. H. Vang, M. Lazar, P. Brosselard, C. Raynaud, P. Cremillieu, J.-L. Leclercq, J.-M. Bluet, S. Scharnholz, and D. Planson, *Superlattices Microstruct.* 40, 626 (2006).
12. L.G. Fursin, J.H. Zhao, and M. Weiner, *Electron. Lett.* 37, 1092 (2001).
13. B. Pécz, G. Radnóczi, S. Cassette, C. Brylinski, C. Arnodo, and C. Noblanc, *Diam. Relat. Mater.* 6, 1428 (1997).
14. T.S. Marinova, A. Kakanakova-Georgieva, V. Krastev, R. Kakanakov, M. Neshev, L. Kassamakova, O. Noblanc, C. Arnodo, S. Cassette, C. Brylinski, B. Pécz, G. Radnoczi, and G. Vincze, *Mater. Sci. Eng.* B46, 223 (1997).
15. R. Liu, *ULSI Technology*, ed. C.Y. Chang and S.M. Sze (Singapore: McGraw-Hill, 1996), p. 371.
16. J.H. Park and P.H. Holloway, *J. Vac. Sci. Technol. B* 23, 486 (2005).
17. R. Pérez, N. Mestres, D. Tournier, P. Godignon, and J. Millán, *Diam. Relat. Mater.* 14, 1146 (2005).

18. T. Ohyanagi, Y. Onose, and A. Watanabe, *J. Vac. Sci. Technol. B* 26, 1359 (2008).
19. P. Macháč, B. Barda, and J. Maixner, *Appl. Surf. Sci.* 254, 1691 (2008).
20. W. Kern and D.A. Puotinen, *RCA Rev.* 31, 187 (1970).
21. E. Oliviero, M. Lazar, H. Vang, C. Dubois, P. Cremilleu, J.L. Leclercq, J. Dazord, and D. Planson, *Mater. Sci. Forum* 556–557, 611 (2007).
22. S.W. Russell, J.W. Strane, J.W. Mayer, and S.Q. Wang, *J. Appl. Phys.* 76, 257 (1994).
23. F. La Via, F. Roccaforte, A. Makhtari, V. Raineri, P. Musemeci, and L. Calcagno, *Microelectron. Eng.* 60, 269 (2002).
24. I.P. Nikitina, K.V. Vassilevski, A.B. Horsfall, N.G. Wright, A.G. O'Neill, C.M. Johnson, T. Yamamoto, and R.K. Malhan, *Semicond. Sci. Technol.* 21, 898 (2006).
25. F. Goesmann and R. Schmid-Fetzer, *Mater. Sci. Eng.* B46, 357 (1997).
26. M. Levit, I. Grimberg, and B.-Z. Weiss, *J. Appl. Phys.* 80, 167 (1996).
27. S.Y. Han, K.H. Kim, J.K. Kim, H.W. Jang, K.H. Lee, N.-K. Kim, E.D. Kim, and J.-L. Lee, *Appl. Phys. Lett.* 79, 1816 (2001).
28. Z. Wang, S. Tsukimoto, M. Saito, K. Ito, M. Murakami, and Y. Ikuhara, *Phys. Rev. B* 80, 245303 (2009).
29. S. Li, Y. Zhou, and H. Duan, *J. Mater. Sci.* 37, 2575 (2002).